Journal of Nanostructure in Chemistry (2021) 11:601–617
https://doi.org/10.1007/s40097-021-00387-9

ORIGINAL RESEARCH

Continuous synthesis of photocatalytic nanoparticles of pure ZnO and ZnO modified with metal nanoparticles

Olga Długosz[1] · **Marcin Banach**[1]

Received: 19 August 2020 / Accepted: 8 January 2021 / Published online: 28 January 2021

Abstract

The continuous microwave synthesis of ZnO, ZnO–nAg and ZnO–nCu nanoparticles (NPs) are presented. Initially, pure ZnO nanoparticles were synthesised, studying the effect of selected parameters on the size of crystallites. In the second stage, ZnO nanoparticles modified with metal nanoparticles were obtained by conducting the process in a flow system. Tannic acid was used as a reducing agent of silver and copper ions. The structure, crystallinity and effectiveness of the deposition of metal nanoparticles were assessed by XRD, XPS, FTIR and electron microscopy techniques (SEM and TEM). The obtained materials were tested for their photocatalytic properties against methylene blue in UV light. The results of photodegradation in ultraviolet light have shown that the introduction of metal nanoparticles, especially silver nanoparticles, significantly increases catalytic efficiency (30% for pure ZnO NPs, 91% for ZnO–nAg NPs and 54% for ZnO–nCu NPs). The main advantage of the proposed ZnO/Ag semiconductor is that it delays the recombination process of electron–hole pairs generated by photon absorption, which extends the efficiency of such a photocatalyst. Based on the research, we determined that it is possible to use photocatalytically active ZnO modified with metal nanoparticles obtained in the flow process.

✉ Olga Długosz
odlugosz@chemia.pk.edu.pl

[1] Faculty of Chemical Engineering and Technology, Institute of Chemistry and Inorganic Technology, Cracow University of Technology, Warszawska St. 24, 31-155 Cracow, Poland

Graphic abstract

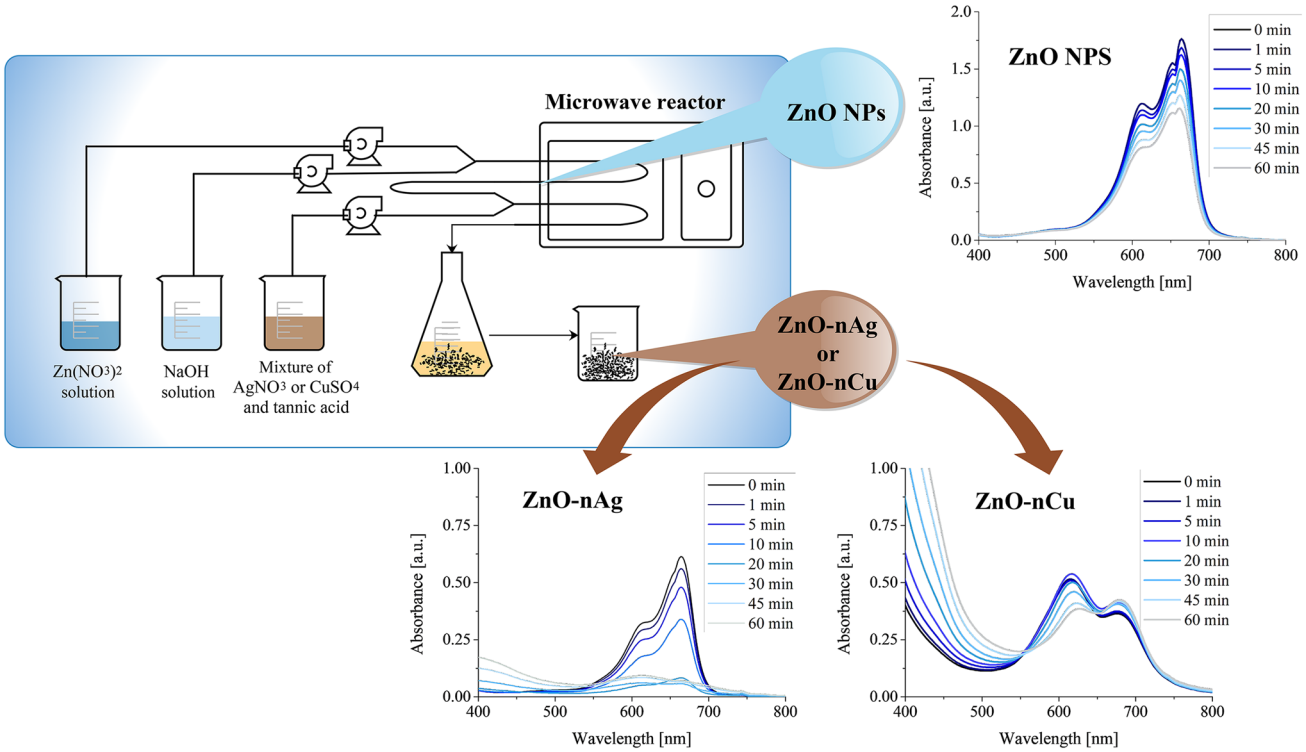

Keywords Photocatalytic activity · ZnO NPs · Metal nanoparticles · Continuous process

Introduction

The possibilities offered by nanometre sized products are vast and potentially meaningful in research and industry [1, 2]. Among inorganic compounds, zinc oxide nanoparticles stand out compared to other commonly used nanomaterials, in view of their photocatalytic activity and antimicrobial properties with a lack of toxicity and high stability [3].

ZnO has a broader energy gap (3.3 eV) compared to TiO_2 (3.15 eV), which directly contributes to lower photocatalytic activity [4, 5]. To improve photocatalytic efficiency, many methods have been proposed for the modification of oxide semiconductors, such as the deposition of noble metal oxides or doping with metal and non-metal ions [6, 7]. The addition of metal nanoparticles on the surface of oxide semiconductors allows the capture of photogenerated electrons and avoids recombination of photogenerated electron–hole pairs [8]. The addition of metal nanoparticles may cause a change in the distance between the conduction and valence band, which decreases the band gap [9]. It was confirmed that the addition of nanoparticles of Ag, Au, Cu, Pt and Pd increases the photocatalytic activity of the base material compared to the unmodified material [10, 11]. The nanoparticles present on the surface of photocatalytic material can act as traps for photoinduced electrons, preventing the recombination of electron–hole pairs [12]. In the case of metal nanoparticles, an important additional mechanism is their catalytic nature, through which they can act as active sites of photocatalytic processes [13–15]. The interaction of Au, Ag or Pd nanoparticles with ZnO, which is an n-type semiconductor, causes modifications of the ZnO energy band at the phase boundary [16]. As a result, a Schottky barrier is created that allows the capture of electrons, making it possible to transfer free electrons between the metal and the semiconductor [17, 18]. Wu et al. [19] investigated the impact of the deposition of noble metal nanoparticles, i.e. Ag and Au, by modifying ZnO NPs. By controlling the concentration of metal nanoparticles in the final product, a material with increased photocatalytic activity was obtained. The results of the experiments showed that the modification of the surface of Au nanoparticles not only made Au-ZnO exhibit a faster degree of degradation, but also effectively inhibits the occurrence of Au-ZnO photocorrosion by improving the cyclic activity of the material.

Among the well-known and commonly used metal nanoparticles, the main representatives are silver and copper. The Ag and Cu nanoparticles show a number of desirable properties, including high antimicrobial activity, catalytic and optical properties [20]. By modifying the zinc oxide surface, the addition of Ag or Cu significantly improves the photocatalytic properties. At the same time, they influence additional parameters of the material, so that the product obtained in this process is multifunctional and can be successfully used as an active ingredient of coatings with photocatalytic properties under visible light and UV and also forms a coating resistant to micro-forming [21]. The properties of metal nanoparticles are influenced both by the proportion of nanoparticles used in the product and the form in which they are introduced, i.e. the shape and size of particles [22]. Abdel Messih et al. [23] confirmed that the limited addition of silver nanoparticles does not sufficiently increase the activity of the whole surface of the photocatalyst, while too high a concentration of nanoparticles may disrupt the process of electron–hole pair generation, shortening the life of the material. It is therefore necessary to select the most favourable concentration of the additive while ensuring that the nanoparticles are evenly distributed over the entire surface of the catalyst.

Next to concentration, the key parameter for a successful catalyst is the form of connection of the components with each other. As a result of nanoparticles settling on the surface of ZnO, the interaction of metal nanoparticles with oxide is possible, thus without producing strong interactions between the particles, the material will lose its stability and effectiveness in time [24, 25]. An alternative to the known processes of obtaining nanocomposites is the use of microwave energy. Microwave energy penetrates inside the system, resulting in the degree of energy use being higher compared to conventional heating [26]. Reactors receive sufficient energy so that the efficiency of Me NPs deposition is high, which extends the future activity of the photocatalyst. Furthermore, the microwave reactor allows the processes to be carried out in a short time.

By combining microwave energy with a continuous process, it is possible to obtain nanomaterials on an increased scale, without losing their physicochemical properties. Continuous demand of the product with ZnO NPs forced chemists to develop efficient methods of nanoparticle synthesis in a large scale [27, 28]. One of the major challenges to produce nanoparticles in a larger scale is the lack of scale periodic process carried out in reactors with conventional heating. Heating the surface of the material causes a lower increase in the processes compared to the increase in volume and ratio of nanoparticles. This phenomenon limits a substantial increase in scaling the procedure for commercial uses. A different approach can be taken by maintaining the scale of the apparatus but by increasing the flow of the reagents [29]. That approach makes it possible to control process parameters that should be constant in the reactor's established operation, which makes it possible to test the quality of the obtained product "in situ". In order to reduce the residence time, it is necessary to supply energy to a system with sufficient power. One of the major methods based on metal hydroxide precipitation processes combined with dehydration results in a metal oxide being obtained. Microwave irradiation allows the process to be carried out without further calcination processes, because the microwave energy is sufficiently high to obtain material with high crystallinity [30].

In this study, ZnO NPs were modified by metal nanoparticle additives. The pure and modified ZnO NPs were synthesised by a precipitate continuous process, using irradiation power as the source of energy. The impact of process parameters such as microwave power, residence time and presence of stabiliser was tested to identify the resulting size of the ZnO NPs. The effect of additive concentration on photocatalytic properties was also investigated.

Materials and methods

Materials

The ZnO NPs was prepared using solutions of zinc nitrate(V) (Sigma Aldrich) and sodium hydroxide (POCH). Glycol polyethylene 400 (PEG) (Sigma Aldrich) solution was used as stabilising agent. The ZnO NPs were modified by additives of silver or copper nanoparticles. For this purpose, a mixture of silver nitrate(V) (Sigma Aldrich) or copper(II) sulphate (Sigma Aldrich) with tannic acid (Sigma Aldrich) were used.

The photocatalytic properties of pure and modified zinc oxide nanoparticles were verified via the photodegradation of Methylene Blue solution (Sigma Aldrich).

The experimental setup—microwave reactor

The processes of metal oxide nanoparticle formation were carried out in a continuous system using a microwave reactor as the source of energy. The method of synthesis of metal oxide nanoparticles was presented in a previous paper [31]. The synthesis of ZnO and ZnO/nMe NPs were carried out in a continuous microwave flow reactor (CMFR). The stream of $Zn(NO_3)_2$ solution was mixed with the NaOH solution stream and the PEG solution stream. In the reactor, in the microwave radiation field, a process of precipitation of zinc hydroxide and a simultaneous dehydration process took place, resulting in a suspension of ZnO NPs. The total flow rate of the solution varied from 171.5 to 516.0 μm^3 /s, depending on the residence time. The volume ratio of

reagents was 5:2.5:2.5 for the metal ions solution, PEG solution and precipitating solution, respectively. The concentration of $Zn(NO_3)_2$ solution equalled 12 g/dm^3 and the concentration of NaOH solution was 13 g/dm^3. The final concentration of metal oxide nanoparticles was 5000 mg/dm^3. The suspension was filtered and the solids were washed and dried at 105 °C, for 24 h to obtain the finished product. The processes of synthesis of ZnO NPs were examined by the following variable parameters: the initial concentration of stabiliser, the residence time, and the irradiation power. The initial PEG concentration was changed in the range of 0–2%$_{mass}$. The residence time of the mixture and the irradiation power were investigated in the ranges of 40–80 s and 300–600 W. As a dependent variable, the size of crystallinity of ZnO was chosen.

An experimental setup for the synthesis of modified ZnO NPs is presented in Fig. 1. The reactor was divided into two zones. During the first step, ZnO NPs were synthesised. The concentration of $Zn(NO_3)_2$ solution was 12 g/dm^3 and the concentration of the NaOH solution was 13 g/dm^3. Next, the stream with a suspension of ZnO NPs was recycled and the stream of the mixture of metal precursor and tannic acid was added. After this process, the suspension contained a metal oxide suspension with metal nanoparticles and was collected and filtered under pressure. The moist product was dried in 105 °C for 24 h. The processes of the synthesis of ZnO NPs modified by silver or copper nanoparticles were examined by the following variable parameters: the initial concentration of metal ions, the molar ratio of tannic acid to metal ions and the irradiation power. The initial salt concentration was changed in the range of 100–500 mg/g in the final photocatalytic material. The irradiation power was investigated in the range of 180–450 W and the molar ratios were changed depending on the metal (nT/nAg = 0.2–0.8 and nT/nCu = 1.2–1.8, respectively for silver and copper additives). As a dependent variable, the concentration of leaching metal nanoparticles in the photocatalysts was chosen.

The effect of the parameters on the size of ZnO crystallinity and the concentration of leaching metal nanoparticles in ZnO–nMe were determined using the CCD (Central Composite Design) plans in combination with ANOVA analysis, using the STATISTICA program.

Instrumental analysis

The crystalline phases of the particles were examined by X-ray diffractometry (XRD) using an X-Pert Pro apparatus (Phillips, Netherlands). The shape and size of the nanoparticles was characterised by transmission electron microscopy (TEM) (Philips CM12 STEM) equipped with an energy dispersive X-ray spectroscope (EDX). Fourier Transform infrared spectra were recorded on an IR Prsestige-21 Schimadzu spectrophotometer. Concentrations of dye solutions were studied using UV–Vis spectrometry (RayLeigh UV-1800). Based on UV–visible diffused reflectance spectrophotometry (UV–Vis-DRS), the band gap value was determined (Shimadzu UV-2450 UV–Visible spectrophotometer). Elemental information of the pure and modified ZnO was recorded by X-ray photoelectron spectroscopy (XPS) (PHI Quantum 2000, Physical Electronics, Inc.).

The crystallite sizes were examined using the XRD method, measuring the Bragg angle. The calculated crystallite size was the starting factor used in the CCD plans. X-Ray diffraction is sensitive to the crystallite size, which can be determined by the Scherrer equation [32]:

$$d = \frac{K\lambda}{\beta \cos \Theta} \tag{1}$$

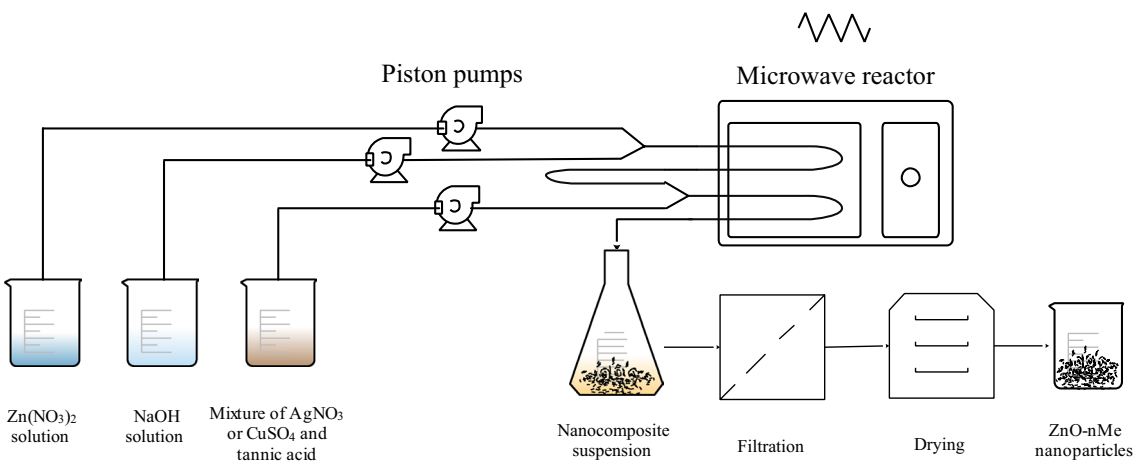

Fig. 1 Scheme of synthesis of ZnO NPs modified by metal nanoparticles

where K—dimensionless shape factor ($K = 0.9$), λ—X-ray wavelength (nm), β—full width of peak at half maximum, Θ—Bragg angle.

Photocatalytic properties of pure and modified ZnO NPs

Effect of the addition of metal nanoparticles on the photocatalytic activity of ZnO

Photocatalytic properties of pure and modified zinc oxide nanoparticles were verified via the photodegradation of a Methylene Blue (MB) solution. For this purpose, 200 mg of the photocatalysts were mixed with 100 cm^3 of the dye solution (20 mg/dm^3 of MB solution). Firstly, each suspension was stirred for 30 min in the dark to obtain sorption equilibrium. Later, samples were stirred under UV light (365 nm). After adequate periods of time, the next samples were collapsed, filtered and the filtrates were analysed using UV–Vis spectroscopy. To identify the concentration of dye in the sample, for each dye a calibration curve was made. Different concentrations of silver or copper nanoparticles were compared against the photocatalytic properties of each dye.

The efficiency of the photodegradation of the dye was used as a value to compare photocatalytic activity:

$$E = \frac{C_0 - C}{C_0} 100\% \tag{2}$$

The rate of the photocatalytic processes was determined using the Langmuir–Hinshelwood kinetic model (L–H model). The linear form of the equation is presented. The k parameter is the proportional coefficient, called the photodegradation rate constant [k (min^{-1})].

$$-\ln\left(\frac{C}{C_0}\right) = kt \tag{3}$$

Stability of the ZnO and modified ZnO NPs

To verify the reproducibility of the ZnO properties and the modified ZnO, a series of tests were carried out in which the effectiveness of dye removal in subsequent cycles was tested. Each 100 cm^3 of 20 mg/dm^3 MB solution was mixed with 200 mg ZnO, ZnO–Ag and ZnO–Cu at 300 rpm. After 30 min in the dark and 60 min in UV light, the suspension was filtered and the material was washed, dried and recycled. At intervals, 2 ml of the suspension was taken to test the concentration of MB over time. The maximum absorbance was determined at 664 nm.

Effects of the scavengers on the mechanism of photodegradation of methylene blue

The 5 cm^3 of solution of the selected scavenger was added to a suspension of 200 mg of material mixed with 100 cm^3 of dye (at an initial concentration of 20 mg/dm^3), while water was added to the neutral sample. After 30 min in the dark and 60 min in UV light the suspension was filtered and the concentration of MB was determined at 664 nm. The following scavengers were compared: triethanolamine, benzoquinone, mannitol and $AgNO_3$, at an initial concentration of 1 mmol/dm^3.

Discussion

The purpose of this research was to develop a continuous method of preparation of ZnO NPs and modified ZnO NPs with enhanced photocatalytic activity. In the first stage, the effect of the process parameters in the synthesis of the pure ZnO NPs was investigated. In the next stage, modification of ZnO NPs using silver and copper nanoparticles was carried out.

Synthesis of ZnO nanoparticles

The results of analysis of process parameters on the size of the crystallite of ZnO NPs are presented in Table 1. The size of particles was changed in the range of 24.79–36.30 nm.

Table 1 Changes in the crystallite size of zinc oxide nanoparticles synthesised in a continuous microwave reactor, under different independent variables

Lp	t (s)	P (W)	C_{stab} ($\%_{mass}$)	nZnO d_{cr} (nm)
1	40	300	0	36.30
2	40	300	2	33.10
3	40	600	0	28.02
4	40	600	2	29.98
5	80	300	0	28.00
6	80	300	2	26.27
7	80	600	0	27.23
8	80	600	2	24.79
9	40	450	1	33.96
10	80	450	1	28.30
11	60	300	1	29.42
12	60	600	1	26.63
13	60	450	0	27.62
14	60	450	2	27.29
15	60	450	1	32.63
16	60	450	1	31.41
17	60	450	1	31.10

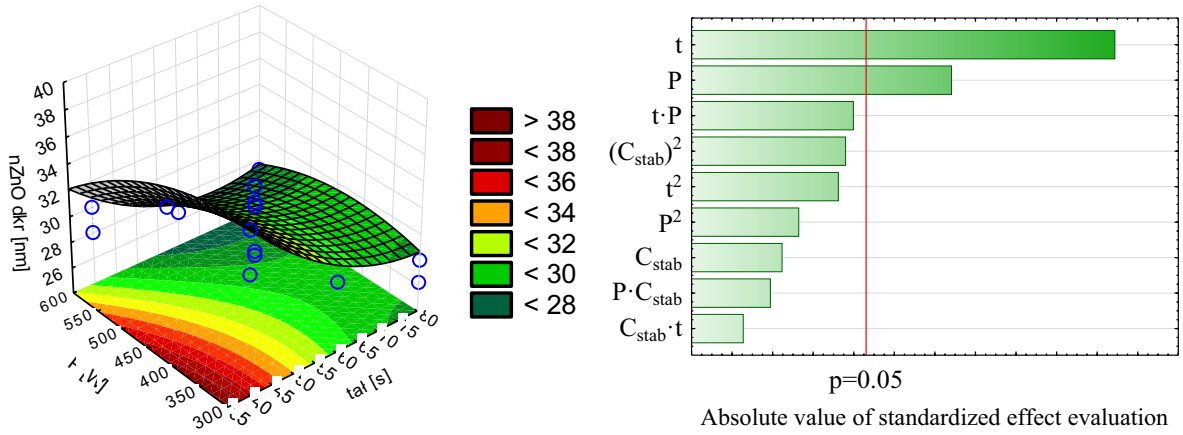

Fig. 2 Impact of parameters of crystallinity size of ZnO NPs with a Pareto plot

Based on the analysis of the influence of the parameters, a significant impact of the residence time of the mixture in the reactor and the microwave irradiation was observed (Fig. 2). An insignificant effect of the stabiliser concentration was observed. Due to the lack of effect from polyethylene glycol addition, in the further stages of the study, the PEG solution was not added.

The reduction of ZnO NPs crystallites is associated with an increase in the surface to volume ratio. Smaller particles have an increased surface area, on which photocatalytic processes will occur. In addition, during surface development, there is an additional increase in the proportion of surface defects that are desirable for photocatalytic processes. The most important parameter turned out to be the reaction time, which results from the possibility of forming larger amounts of smaller crystallites. After exceeding the residence time of the mixture in the reactor for 50 s, a reduction in the crystallite size (below 30 nm) can be observed, despite the increase in microwave radiation. The increase in microwave radiation caused an increase in the crystallinity of the obtained nanoparticles, in addition, the supplied energy prevented their excessive build-up. Barreto et al. obtained ZnO NPs in a microwave reactor, studying among others, the impact of reaction time and the irradiation power. By changing the power value from 300 to 1200 W, it was observed that the formation of aggregates is favoured as the microwave power increases. When the power equals 1200 W, the generation of agglomerates with higher polydispersity can be seen, more so than in comparison to that obtained at 600 W [33].

Synthesis of ZnO NPs modified by Ag/Cu nanoparticles

The processes of synthesis of ZnO NPs modified with silver (ZnO–nAg) or copper (ZnO–nCu) nanoparticles were carried out in a two-stage microwave flow reactor. The residence time of the mixture in the reactor was carried out for 120 s. The microwave irradiation power, the molar ratio of tannic acid to metal ions and the initial concentration of silver or copper ions were selected as parameters that may affect the process of metal nanoparticle deposition (Table 2). After the processes, the suspension containing ZnO NPs with deposited nanoparticles was filtered, and the filtrate was subjected to atomic absorption spectroscopy to check the degree of loss of metal nanoparticles from the material. The results of the impact of individual parameters on the degree of nanoparticle attachment to ZnO are shown in Fig. 3.

Based on statistical analysis, a significant impact of all input parameters was found. It can be seen that depending on the initial concentration of metal ions, the efficiency of nanoparticle deposition on the metal oxide was a maximum of 99.98% and 99.07% for silver and copper nanoparticles, respectively. For all systems, the increase in the concentration of deposited nanoparticles resulted in an increase in the efficiency of depositing particles on ZnO. For materials with a higher content of metal nanoparticles, they can agglomerate, preventing their removal from the final product. When silver nanoparticles were added, an increase in the stabilising agent concentration resulted in an increase in the deposition efficiency of nanoparticles on ZnO. For the deposition of copper nanoparticles, a molar ratio of tannic acid to copper ions of 1.2 minimises the degree of copper ion removal. A further increase in the ratio of tannic acid may cause the formation of copper nanoparticle agglomerates in combination with tannic acid, which have a lower affinity for the ZnO surface.

Analysis of the impact of microwave radiation on the efficiency of deposition of metal nanoparticles on oxide, showed a different effect depending on the added metal. On one hand, the increase in microwave radiation power improves the binding energy efficiency between metal oxide nanoparticles, which thereby increases the efficiency of

Table 2 The efficiency (E) of the metal nanoparticles deposition onto the surface of ZnO NPs synthesised in a continuous microwave reactor under different independent variables

Nr	ZnO–nAg NPs					ZnO–nCu NPs				
	P (W)	C_{nAg} (mg/g)	nT/nAg	C_{Ag^+} (mg/g)	*E (%)*	*P (W)*	C_{nu} (mg/g)	nT/nCu	$C_{Cu^{2+}}$ (mg/g)	*E (%)*
1	180	40	0.2	38.38 ± 2.40	95.95	180	40	1.2	29.72 ± 19.82	74.30
2	180	40	0.8	30.76 ± 2.79	76.90	180	40	1.8	38.38 ± 1.55	95.96
3	180	200	0.2	198.66 ± 1.87	99.33	180	200	1.2	174.83 ± 6.59	87.08
4	180	200	0.8	199.86 ± 0.34	99.93	180	200	1.8	115.01 ± 17.32	57.55
5	450	40	0.2	38.04 ± 4.71	95.10	450	40	1.2	34.64 ± 2.80	86.61
6	450	40	0.8	9.972 ± 4.35	24.93	450	40	1.8	29.36 ± 7.82	73.40
7	450	200	0.2	197.62 ± 1.80	98.81	450	200	1.2	199.63 ± 0.48	99.07
8	450	200	0.8	199.96 ± 0.05	99.98	450	200	1.8	180.76 ± 3.17	91.90
9	180	120	0.5	118.72 ± 2.80	98.93	180	120	1.5	118.00 ± 2.00	95.00
10	450	120	0.5	116.94 ± 0.80	97.45	450	120	1.5	118.64 ± 0.60	96.59
11	300	40	0.5	30.85 ± 11.25	77.13	300	40	1.5	27.76 ± 4.92	69.39
12	300	200	0.5	199.68 ± 0.50	99.84	300	200	1.5	145.39 ± 6.08	73.48
13	300	120	0.2	67.20 ± 119.0	56.00	300	120	1.2	118.46 ± 0.73	96.93
14	300	120	0.8	108.11 ± 13.20	90.09	300	120	1.8	112.63 ± 1.21	81.14
15	300	120	0.5	119.88 ± 0.11	99.90	300	120	1.5	118.63 ± 0.46	96.57
16	300	120	0.5	118.42 ± 1.99	98.68	300	120	1.5	116.82 ± 0.96	92.08
17	300	120	0.5	119.76 ± 0.32	99.80	300	120	1.5	118.13 ± 0.62	95.32

nanoparticle deposition. On the other hand, the increase in radiation power causes a decrease in the crystallite size of the ZnO obtained. Due to their smaller size, copper nanoparticles deposited on the obtained zinc oxide structures at higher power levels. In the case of silver nanoparticles, monodisperse particles with a diameter above 20 nm were obtained, whose deposition efficiency decreased with the increase in radiation power. The increase in power reduced the size of ZnO crystallites by inhibiting the deposition of silver particles.

Effect of stabilising agent concentration

A high impact of all input parameters was found based on statistical analysis. In the case of the addition of silver nanoparticles, an increase in the concentration of the stabilising agent caused a decrease in the concentration of metals in the filtrate. In the case of copper nanoparticle deposition, the molar ratio of tannic acid to copper ions equal to 1.5 minimised the degree of copper ion removal. The highest proportion of tannic acid can cause the formation of agglomerates of copper nanoparticles combined with tannic acid, with a lower affinity for deposition on the surface of ZnO. The beneficial effect of the stabiliser on the inhibition of the release of metal ions has been confirmed in previous studies [34, 35]. Depending on the presence of stabiliser, particles of different sizes can be obtained and an increased ion affinity to the surface can be achieved, preventing changes in the product morphology [36].

Effect of microwave irradiation

Analysis of the impact of microwave radiation on the efficiency of the deposition of metal nanoparticles on oxide, showed a different effect depending on the added metal. The increase in radiation power causes a decrease in the crystallite size of the ZnO obtained. Copper nanoparticles, due to their smaller size, deposited on the obtained zinc oxide structures at higher powers. In the case of silver nanoparticles, higher dispersion particles were obtained with a particle size also above 20 nm, which were deposited to a lower degree at a lower power when ZnO of larger sizes were obtained. Swarnavalli et al. confirmed the possibility of obtaining Ag-modified ZnO NPs using microwave radiation. The efficiency of nitrobenzene degradation was 98% after 100 min, i.e. 2.9 times more than pure ZnO, which only shows 33.6% degradation by the end of 120 min [25].

Effect of initial concentration of silver or copper ions

The increase in the initial concentration of the metal ion solution precursor of silver or copper ions resulted in better deposition of the formed nanoparticles on the ZnO surface, which resulted in a lower concentration of metal ions in the filtrate. An increase in the concentration of metal ions simultaneously caused an increase in the concentration of tannic acid, which bound the resulting metal nanoparticles to the oxide. Kadam et al. confirmed that the Cu content in modified ZnO NPs improved MO

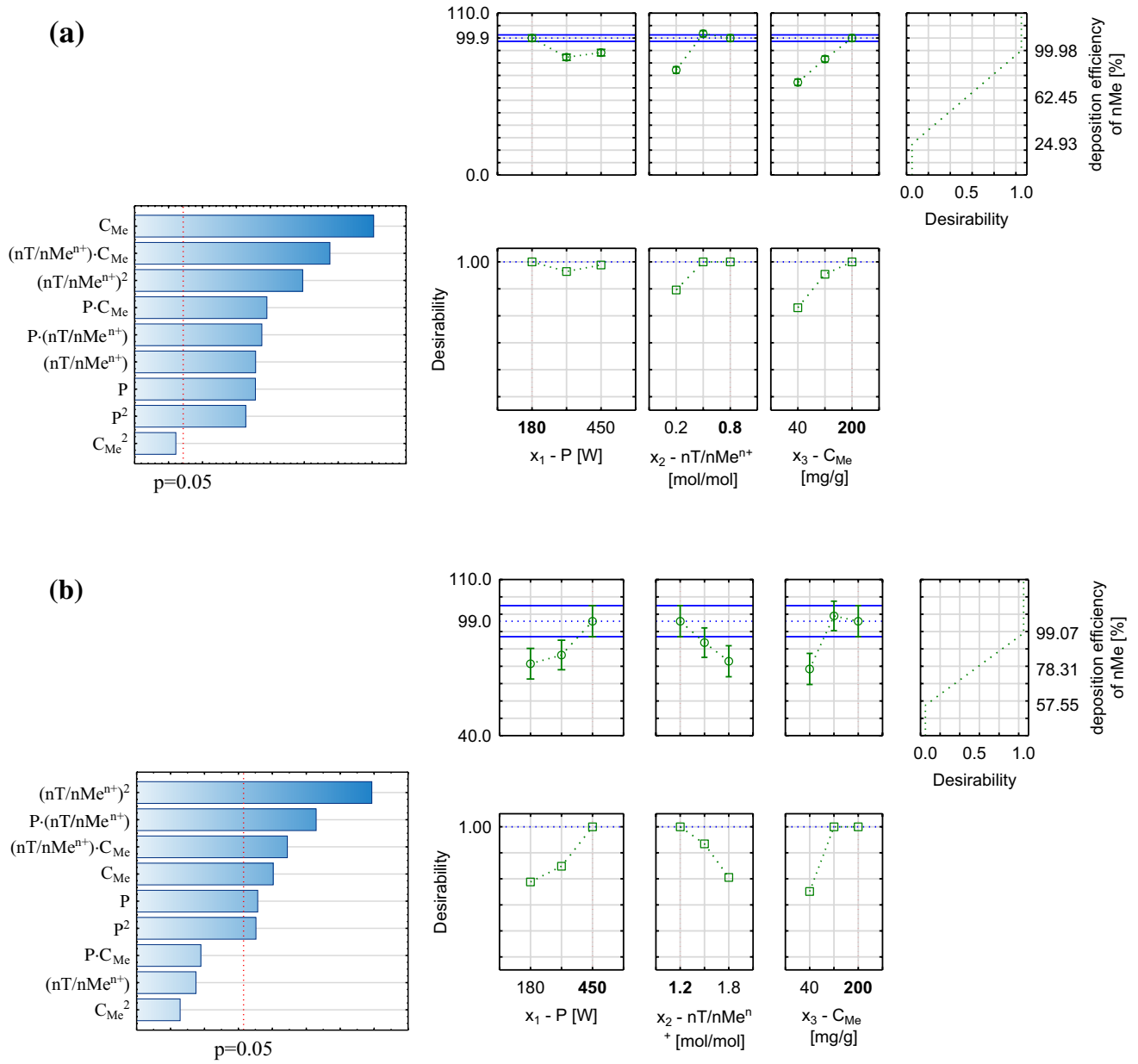

Fig. 3 Impacts of parameters on the deposition of the metal nanoparticles onto the surface of ZnO NPs: **a** ZnO–nAg NPs, **b** ZnO–nCu NPs

photodegradation efficiency to 96, 99.5 and 96%, respectively, for 0.25, 0.50 and 0.75% Cu in ZnO–nCu NPs, whereas for pure ZnO, the efficiency was 74% [37]. The influence of the Ag content on the photocatalytic properties of ZnO was studied by Babar et al. By changing the Ag concentration from 0.25 to 1% mass in ZnO, it was found that the increase in the metal content on the ZnO surface initially improved the ZnO photocatalytic activity. After reaching a certain value, there was a slightly reduced efficiency of MO photodegradation. The best results were obtained for an Ag content of 0.75% ZnO. When Ag deposition is greater than its optimal content, the particles cover a larger area of ZnO and inhibit the absorption of UV radiation between Ag NPs and ZnO [38].

Instrumental analysis of pure and modified ZnO NPs

FTIR measurements were carried out to compare the chemical composition of the obtained materials based on ZnO NPs (Fig. 4). The band around 3500 and 3380 cm^{-1} can be assigned to the O–H stretching vibration, indicating the presence of a hydroxyl group. For pure ZnO NPs, only the band at 1560 cm^{-1} and 1400 cm^{-1} were attributed to the bending vibration of –OH groups and C–H bending, respectively.

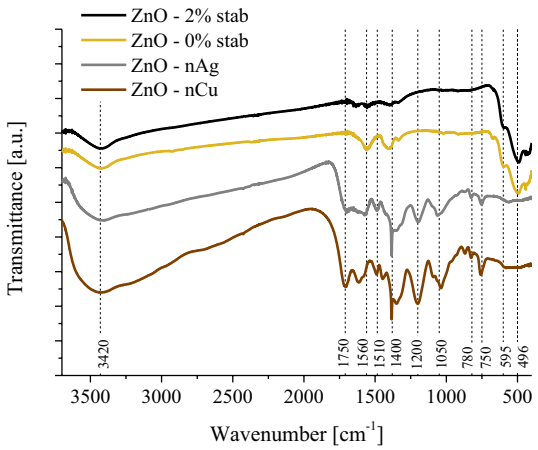

Fig. 4 FTIR diagram for pure ZnO NPs and ZnO modified by metal nanoparticles (ZnO NPs: $P = 450$ W, $t = 60$ s, $C_{stab} = 0\%_{mass}$ and $C_{stab} = 2\%_{mass}$, ZnO–nAg NPs: $P = 300$ W, $t = 120$ s, $C_{Ag^+} = 120$ mg/g, nT/nAg = 0.5, ZnO–nCu: $P = 300$ W, $t = 120$ s, $C_{Cu^{2+}} = 120$ mg/g, nT/nCu = 1.5)

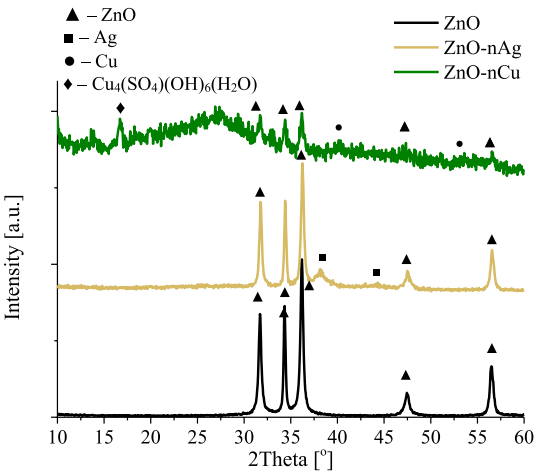

Fig. 5 The XRD diffraction patterns of ZnO NPs, pure and modified by metal nanoparticles (ZnO NPs: $P = 450$ W, $t = 60$ s, $C_{stab} = 2\%_{mass}$, ZnO–nAg NPs: $P = 300$ W, $t = 120$ s, $C_{Ag^+} = 120$ mg/g, nT/nAg = 0.5, ZnO–nCu: $P = 300$ W, $t = 120$ s, $C_{Cu^{2+}} = 120$ mg/g, nT/nCu = 1.5)

Additionally, peaks assigned to metal oxygen bonds at 490 and 440 cm^{-1} were confirmed [39]. ZnO NPs modified with metal nanoparticles have no peaks due to the Me–O bonds, compared to zinc oxide. Tannic acid can cover ZnO NPs. The peaks at the wavenumber between 1750 and 800 cm^{-1} are characteristic of tannic acid [40, 41].

Figure 5 presents results of XRD analysis for ZnO NPs synthesised in microwave reactor at 450 W. Phase analysis revealed that pure zinc oxide with a zincite structure was present. The diffractogram confirmed the presence of a peak at the following 2θ: 31.77 (100), 34.41 (002), 36.26 (101), 47.54 (012), 56.59 (110) [42]. The narrow diffraction peaks of the ZnO pattern indicated a good crystallinity of the material [43]. The characteristic peaks were present both in pure and modified materials. In the XRD pattern of ZnO–nAg, the presence of peak characteristic for silver was observed [12]. The intensity of peaks from the zinc oxide structure were similar and the addition of tannic acid did not change the structure of the basic zinc oxide. In the case of zinc oxide modified with copper nanoparticles, the background is clearly raised, which is associated with high ratio of tannic acid. No peaks corresponding to CuO or Ag_2O phases were observed, whereas impurities of the hydrated copper sulphate phase were confirmed [44].

Figure 6 presents SEM and TEM microphotographs of ZnO (Fig. 6a–c), ZnO–nAg (Fig. 6d–f) and ZnO–nCu (Fig. 6g–i). The particles had an irregular shape, but were slightly spherical. In the preparation of ZnO–nAg NPs, the deposition of polydisperse particles of a spherical shape can be observed (Fig. 6f). In the case of ZnO–nCu modification based on the EDX method, the presence of carbon derived from tannic acid can be observed (Fig. 6i). The deposited copper nanoparticles are characterised by being highly monodispersed.

The band gaps for pure ZnO NPs were calculated as 3.20 eV. The influence of nAg and nCu deposition on the metal oxide band gap was observed by surface analysis of differential reflectance spectroscopy (DRS). The addition of the metal nanoparticles reduced the energy band gap to 3.00 eV for ZnO–nAg NPs and to 3.15 eV for ZnO–nCu NPs. The change of the band gap was associated with deposition of metal nanoparticles on the surface of ZnO nanoparticles. Electrons from Ag and Cu are transferred to the surface of ZnO leading to a reduced energy band gap, thus improving the photocatalytic efficiency of the nanocomposites. Karimi-Maleh et al. [45] confirmed the decreasing band gap of the ZnO NPs after the addition of silver nanoparticles. The 3% nAg addition reduced the band gap of ZnO NPs from 3.20 to 2.78 eV. Figure 7 presents diffuse reflectance (DRS) spectrum of the ZnO, ZnO-nAg and ZnO-nCu NPs.

The XPS analysis was carried out to determine the surface composition and oxidation status of elements present in ZnO NPs, ZnO–nAg NPs and ZnO–nCu NPs (Fig. 8). Two peaks at 1020.3 and 1043.3 eV were attributed to the Zn 2p3/2 and Zn 2p1/2, respectively. The difference between the two Zn peaks confirmed 2 + oxidation state of zinc (Fig. 8a). In combination with the O1s peak detection at 531.5 eV, can be found to obtain ZnO [46]. Figure 8b, c present XPS ZnO–nAg NPs and ZnO–nCu NPs spectra. On the surface of nanocomposites Zn, O, Ag and Cu profiles were observed. In ZnO–nAg nanocomposite, the peaks of Ag 3d5/2 and Ag 3d3/2 are at 367.7 eV and 373.7 eV, which confirmed the formation of Ag(0) nanoparticles. The addition of Ag to ZnO had no effect on the

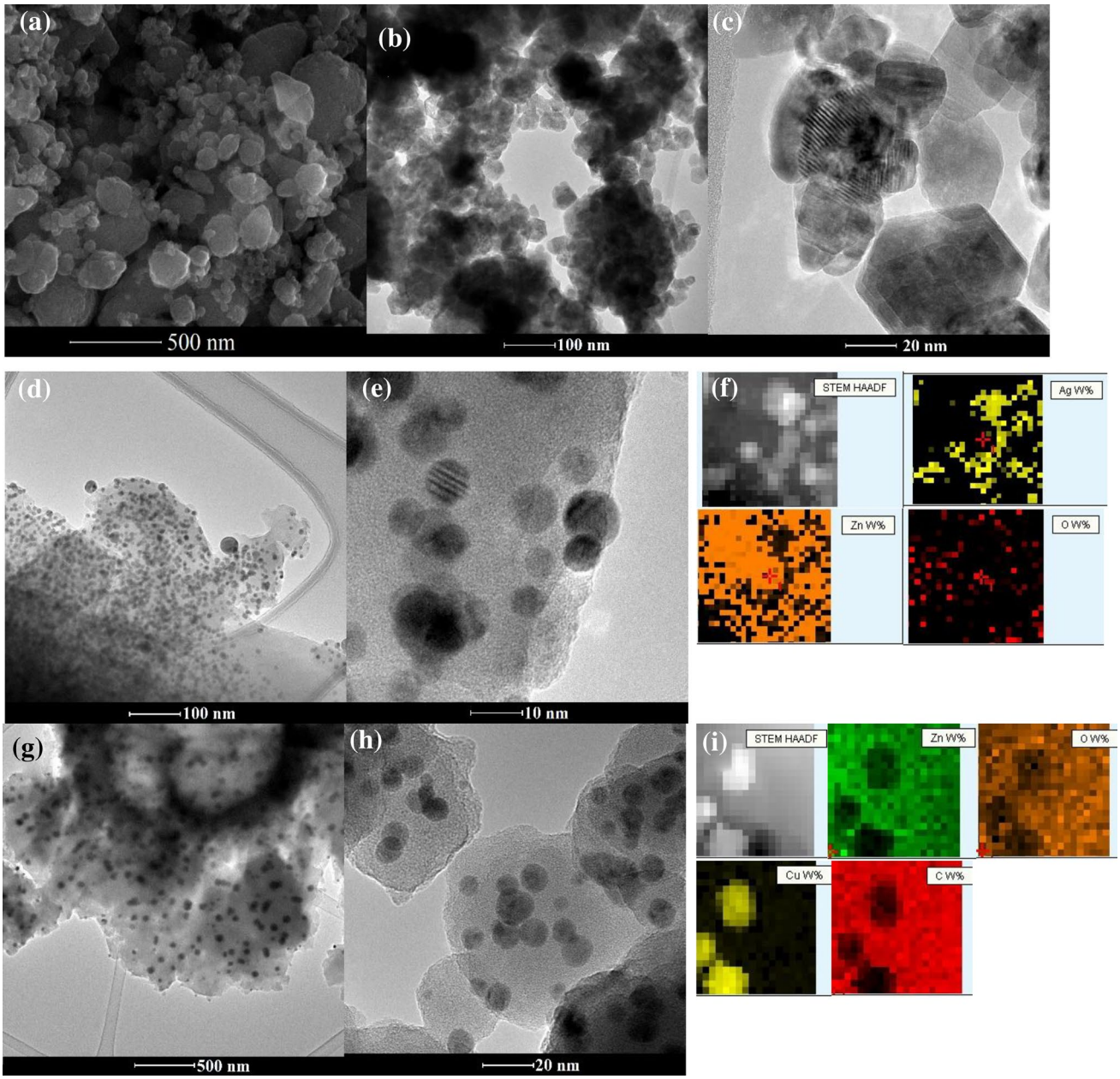

Fig. 6 **a** SEM and **b**, **c** TEM microphotographs of pure ZnO NPs (synthesised in $t = 60$ s, $P = 450$ W, $C_{stab} = 1\%_{mass.}$), **d**, **e**, **f** TEM with EDX microphotographs of ZnO–nAg (synthesised in $P = 300$ W, $t = 120$ s, $C_{Ag^+} = 120$ mg/g, nT/nAg = 0.5), **g**, **h**, **i** TEM with EDX microphotographs of ZnO–nCu (synthesised in $P = 300$ W, $t = 120$ s, $C_{Cu^{2+}} = 120$ mg/g, nT/nCu = 1.5)

chemical status of ZnO nanoparticles compared to pure ZnO. The peaks of Cu2p1/2 and Cu2p3/2 are grouped around 933.6 and 948.1 eV, respectively. The occurrence of Cu 3p peak at 83.1 eV was also confirmed, which indicated the formation of CuO beside Cu(0) on the ZnO surface [47]. For ZnO–nCu NPs the peaks attributed to ZnO were lower, additionally the occurrence of O 1 s and C 1 s peaks was observed due to high concentration of the tannic acid introduced into the system [45].

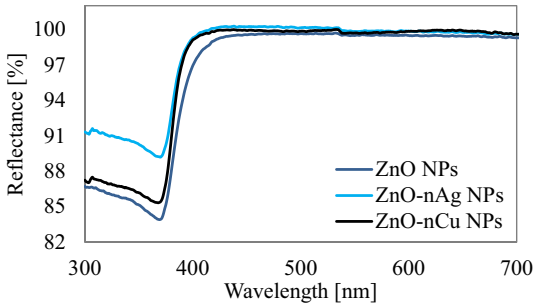

Fig. 7 DRS spectrum of the pure ZnO NPs ($P=450$ W, $t=60$ s, $C_{stab}=0\%_{mass}$), ZnO–nAg NPs ($P=300$ W, nT/nAg=0.5, $C_{Ag^+}=120$ mg/g), and ZnO–nCu NPs ($P=300$ W, nT/nCu=1.5,=$C_{Cu^{2+}}$ 120 mg/g)

Photocatalytic properties of pure and modified ZnO NPs

Analysis of pure ZnO compared to ZnO modified with metal nanoparticles showed a lower absorbance in the case of MB (Fig. 9). For copper nanoparticles, the MB photodegradation efficiency increased by 24% by using a concentration of 120 mg/g nCu on the surface of the ZnO NPs. Similarly, when using ZnO–nAg, the best concentration turned out to be 120 mg/g Ag. With the addition of silver nanoparticles, the efficiency of the bed was significantly higher and exceeded 90% after 60 min of the process.

The Langmuir–Hinshelwood model showed a good fit to the experimental points. By analysing the kinetics of MB photodegradation processes, constants of dye degradation rates and the degree of fit of the model to the data were determined (Table 3). When comparing the addition of silver nanoparticles with copper nanoparticles, it can be observed that for ZnO–nCu materials, photodegradation constants reach higher values. Due to the above, the degree of removal over time should be the highest, which can be assumed as a result of the rapid recombination process of electron–hole pairs; this means that the material with the addition of copper nanoparticles is deactivated, limiting further photocatalysis. In addition, in the case of copper nanoparticles, they can be gradually agglomerated in an aqueous environment. In the case of materials with the addition of silver nanoparticles, higher photocatalytic efficiencies can be observed compared to that occurring from the addition of nCu, regardless of the concentration of nanosilver. This may indicate a slower recombination process for electron–hole pairs. In addition, the high stability of silver nanoparticles can facilitate electron transport, thereby increasing the activity of the photocatalytic process.

Experimental points along with the adjustment of the photodegradation process of MB on ZnO modified with metal nanoparticles is shown in Fig. 10.

Photodegradation studies on MB for ZnO and ZnO with the addition of Ag were conducted by Phuruangrat et al.

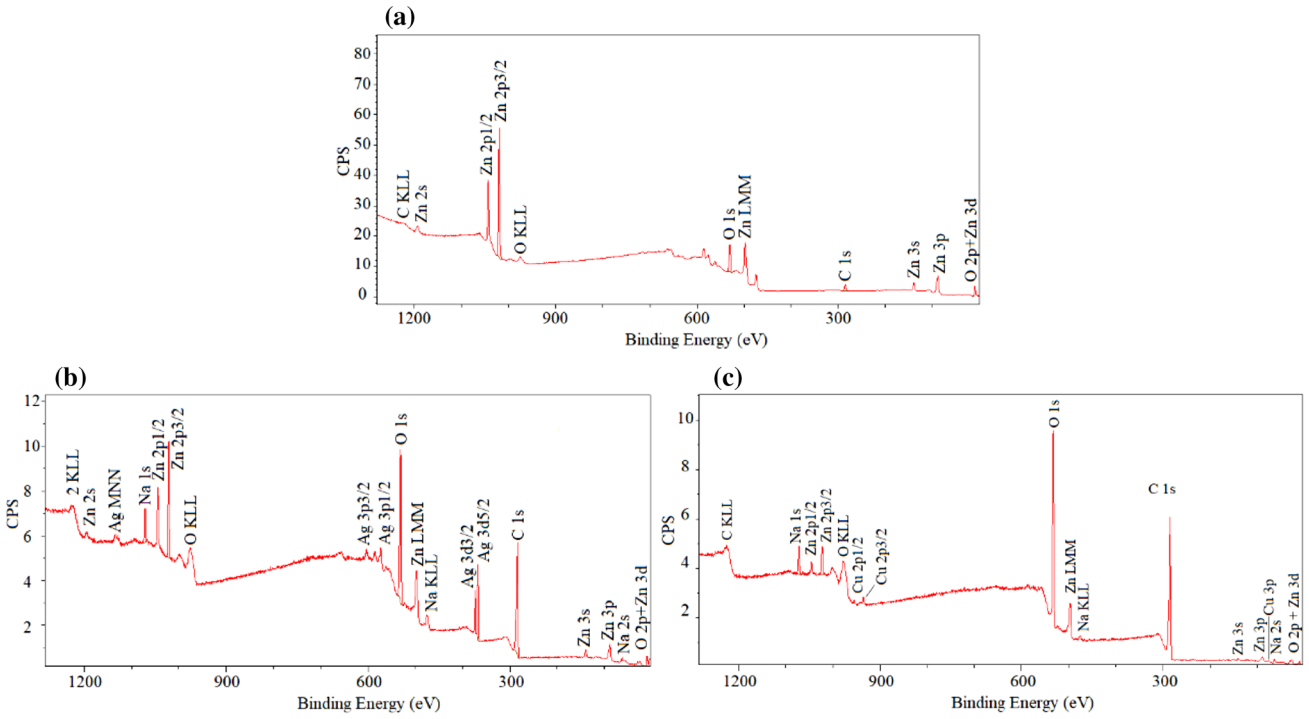

Fig. 8 XPS analysis of pure and modified ZnO NPs: **a** ZnO ($P=450$ W, $t=60$ s, $C_{stab}=0\%_{mass}$), **b** ZnO–nAg ($P=300$ W, nT/nAg=0.5, $C_{Ag^+}=120$ mg/g), **c** ZnO–nCu ($P=300$ W, nT/nCu=1.5, $C_{Cu^{2+}}=120$ mg/g)

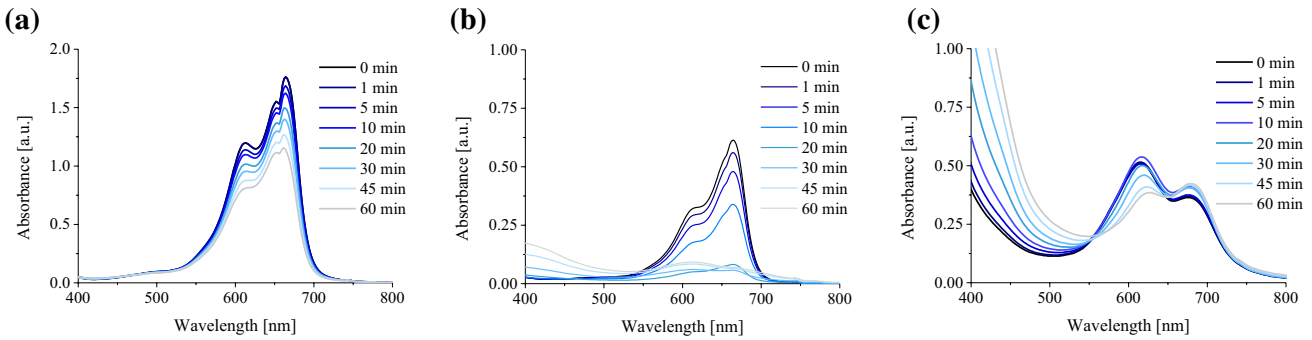

Fig. 9 UV–Vis spectrum for the photodegradation of Methylene Blue (MB): **a** ZnO NPs (synthesised in $P = 450$ W, $t = 60$ s, $C_{PEG} = 0\%_{mass}$), **b** ZnO–nAg NPs (synthesised in $P = 300$ W, $t = 120$ s, $C_{Ag^+} = 120$ mg/g, nT/nAg = 0.5), ZnO–nCu NPs (synthesised in $P = 300$ W, $t = 120$ s, $C_{Cu^{2+}} = 120$ mg/g, nT/nCu = 1.5)

Table 3 The parameters of Langmuir–Hinshelwood kinetic equations for photodegradation of dye solutions onto ZnO NPs, b) ZnO–nAg NPs and ZnO–nCu NPs

Photocatalyst	ZnO NPs	ZnO–nAg NPs			ZnO–nCu NPs		
C_{Me}(mg/g)	0	40	120	200	40	120	200
Number sample		(11)	(15)	(12)	(11)	(15)	(12)
k constant (min^{-1})	0.006523	0.006951	0.01295	0.008911	0.005318	0.01339	0.005683
R^2 coefficient	0.9641	0.9356	0.9356	0.9907	0.9577	0.9235	0.7839
Efficiency after 60 min (%)	30.19	42.52	91.23	76.58	27.83	54.20	32.53

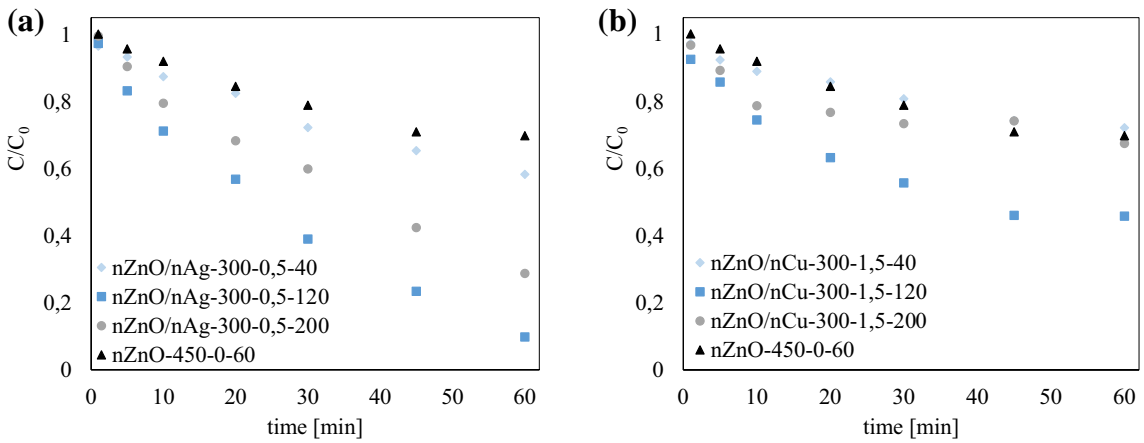

Fig. 10 Kinetics of photocatalyst degradation of MB under UV radiation: **a** ZnO–nAg NPs, **b** ZnO–nCu NPs

[24] Pure ZnO showed a photocatalytic efficiency of 42%. The addition of $10\%_{mass}$ Ag nanoparticles increased the composite efficiency to 96%. The photodegradation rate constant for $1\%_{mass}$ Ag was $5.05 \cdot 10^{-3}$ min^{-1}, which is in accordance with values obtained in the presented studies. Kadam et al. [37] studied the photocatalytic activity of ZnO with the addition of copper nanoparticles, relative to Orange Methyl in UV light. It was confirmed that the increase in copper content to 0.5 mol% Cu resulted in the highest degree of photodegradation. The photodegradation rate changed from 0.01381 to 0.03887 min^{-1} from a copper content of $0.25–0.50\%_{mol}$ Cu, whereas for $0.75\%_{mol}$ it decreased ($k = 0.0268$ min^{-1}). The results obtained in the study were compared with other materials used for photodegradation of dyes (Table 4).

Table 4 Comparison of the photodegradation efficiency of methylene blue on pure ZnO and modified ZnO NPs

Nr	Material	Light	Effectiveness (%)	References
1	ZnO ZnO–Fe(2%)	UV	86 92	[48]
2	ZnO–Ag(3%)	UV Visible	96 56	[23]
3	ZnO with *Kalopanax septemlobus*	UV	97.5	[49]
4	ZnO ZnO–La(3%)	UV	65 80	[50]
5	ZnO ZnO–GO	UV	49 98.5	[51]
6	rGO/ZnO/Cu	UV	95.14	[52]
7	ZnO ZnO/Au(10%)/Pd(5%)	Visible	39 97	[53]
8	ZnO–Cu	UV	60	[54]
9	ZnO ZnO–Au	UV	64.3 82.1	[55]
10	ZnO ZnO–Ag ZnO–Au	UV	8 45 25UV	[56]
11	ZnO ZnO–Ag ZnO–Cu	UV	30.19 91.23 54.20	This study

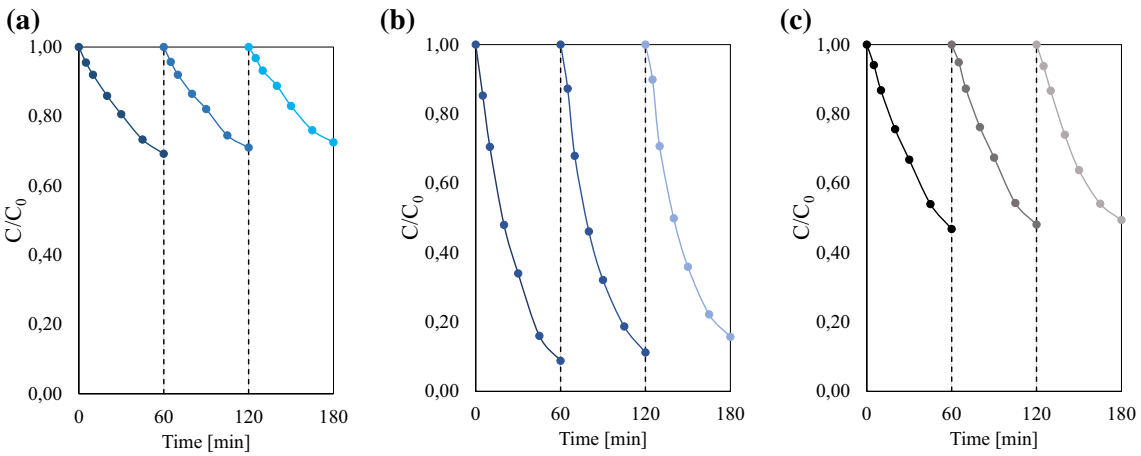

Fig. 11 Recycle efficiency of the photocatalysts during MB photodegradation: **a** ZnO ($P=450$ W, $t=60$ s, $C_{stab}=0\%_{mass}$), **b** ZnO–nAg ($P=300$ W, nT/nAg = 0.5, $C_{Ag^+}=120$ mg/g), **c** ZnO–nCu ($P=300$ W, nT/nCu = 1.5, $C_{Cu^{2+}}=120$ mg/g)

Recyclability of the materials

As a result of the effectiveness of MB degradation in three subsequent work cycles, the high stability of the materials was confirmed (Fig. 11). The decrease in MB degradation efficiency was 3.3%, 6.9% and 3.6% for ZnO, ZnO–nAg and ZnO–nCu NPs, respectively. A higher decrease in process efficiency was observed for the modified materials, which was due to the gradual leaching of metal nanoparticles.

Effects of scavengers

On the basis of the studies around ZnO materials, a significant influence of hydroxyl radicals (•OH) and the presence of holes on the effectiveness of dye degradation was observed (Fig. 12). For ZnO–nAg and ZnO–Cu materials, the presence of hole scavengers reduced the material efficiency. Additionally, for ZnO–nCu and ZnO–nAg superoxide anions, the concentration of hydroxyl radical scavengers had the greatest influence. A significant influence of hydroxyl radicals is associated with the formation of strong oxidants reacting with dye particles. Holes in the valence

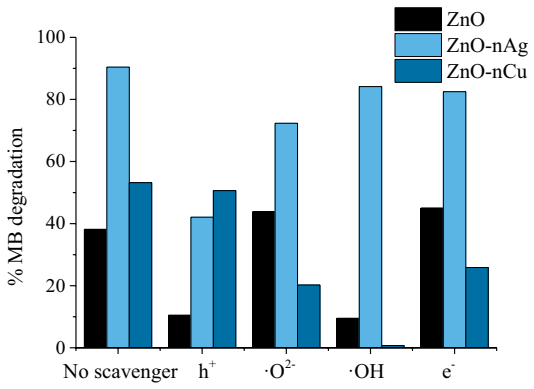

Fig. 12 Photodegradation of MB and RB solutions under different scavengers (C_{AgNO3} = 1 mMol, C_{TEOA} = 278 1 mMol, C_{mannit} = 1 mMol, C_{BQ} = 0.5 mMol, irradiation time 60 min) in the presence of ZnO NPs (P = 450 W, t = 60 s, C_{stab} = 0%$_{mass}$), ZnO–nAg NPs (P = 300 W, nT/nAg = 0.5, C_{Ag} = 120 mg/g) and ZnO–nCu NPs (P = 300 W, nT/nCu = 1.5, C_{Cu} = 120 mg/g)

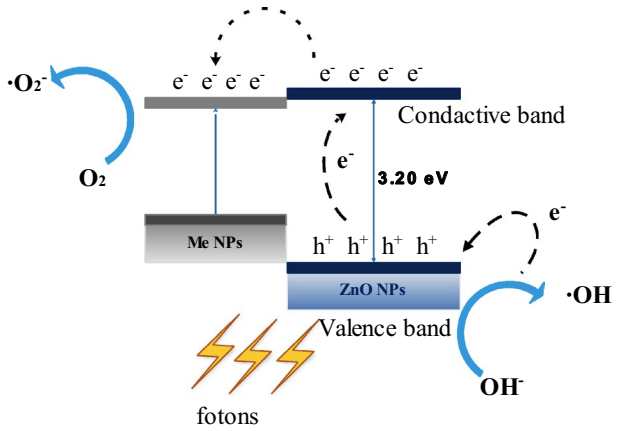

Fig. 13 The photocatalytic mechanism of the electron–hole pair separation of ZnO–nMe NPs in the degradation of MB

band can react with hydroxyl molecules on the surface to form hydroxyl radicals, which are extremely powerful oxidants which can react with organic chemicals [57].

Mechanisms of photodegradation processes

In the analysis of dye photodegradation processes, the initial stage is the sorption of dye particles on the photocatalyst. Adsorption of particles enables the interaction between the catalyst and degraded material. Ultraviolet radiation acting on the nanoparticles of zinc oxide creates a source of photons with an energy equal to or greater than the band gap of ZnO. Electrons (e^-) in the valence band (VB) are excited to the conduction band (CB), while generating the same number of holes (h^+). The electrons from the conduction band migrate to metal particles and can be transferred to oxide particles adsorbed on the ZnO surface, forming free radicals: $\bullet O_2^-$, $\bullet HO_2$, $\bullet OH$, etc., (Fig. 13). The analysis of the scavengers' influence on the efficiency of photodegradation confirmed the importance of the formation of holes where hydroxyl radicals are formed.

The addition of both types of metal nanoparticles reduces the width of the energy gap of the entire material. In the case of ZnO modification with copper nanoparticles, oxygen vacancy trap centres formed, which caused the formation of electrons [44]. Oxygen adsorbed on copper nanoparticles created superoxide anion ($\bullet O_2^-$) radicals by combining with the resulting electrons. In turn, the holes formed on the ZnO surface reacted with the adsorbed hydroxyl ions to form hydroxyl ($\bullet OH$) radicals. When silver nanoparticles were added, defects formed at the Ag–ZnO junction, suppressing charge recombination by transferring photogenerated electrons to the dye in solution [6]. Active radicals reacting with dissolved dye molecules caused their gradual degradation to simpler forms [58]. In the initial stages, the least stable bonds decay, resulting in single ring compounds, which in the final stage become basic inorganic compounds like H_2O, CO_2, NO_3^- and SO_4^{2-} [59]. The mechanism of dye photodegradation using a ZnO semiconductor, initiated by UV, can be presented in the following equation:

$$ZnO + hv \rightarrow ZnO\left(h^+ + e^-\right)$$

$$h^+ + OH^- \rightarrow \cdot OH$$

$$h^+ + H_2O \rightarrow \cdot OH + H^+$$

$$Ag \leftrightarrow Ag^+ + e^-$$

$$e^- + O_2 \rightarrow \cdot O_2^-$$

$$\cdot O_2^- + H^+ \rightarrow \cdot OH_2$$

$$2 \cdot OH_2 \rightarrow H_2O_2 + O_2$$

where h^+ are holes of the generated valence band of the ZnO, which have strong oxidising properties, and e^- are electrons generated in the conduction band of the ZnO, which have high reducing properties [60]. Fageria et al. [46] compared ZnO modified nanoparticles of Au and Ag and proposed a way to increase the ZnO photocatalytic activity as a result of the formation of a Schottky barrier between materials with different work functions. Au and Ag nanoparticles effectively adsorb electrons from the conduction band, and thus prevents the immediate recombination process. Here, Au and Ag nanoparticles are used as surface traps, which usually capture electrons from the ZnO surface and

use them to degrade the dye. A subsequent electron transfer would be beneficial for the proper formation of connections between ZnO and metal nanoparticles. Therefore, embedded metal nanoparticles can act as an electron absorber or an electron trap on the surface of ZnO particles.

Conclusion

This research presented a method of obtaining ZnO NPs, carried out in a flow microwave reactor. The method allowed the possibility of simultaneous synthesis of zinc modified with silver or copper nanoparticles. The materials were characterised by increased photocatalytic activity. The change of the process input parameters, including the power of microwave radiation and the residence time of the mixture in the reactor, allowed us to change the crystallite size of the obtained ZnO NPs. Depending on the selection of the initial concentration of the solution of metal ions that are precursors of metal nanoparticles and also the concentration of the reducing-stabilising factor, it is possible to obtain a material with increased photocatalytic activity compared to pure zinc oxide. The addition of copper nanoparticles or silver nanoparticles improved the photocatalytic efficiency of the photodegradation of MB. The photocatalytic activity of zinc oxide increased from 30 to 91% by modifying its surface with Ag nanoparticles and to 54% by modifying with Cu nanoparticles.

Funding This research did not receive any specific grant from funding agencies in the public, commercial, or not-for-profit sector.

Compliance with ethical standards

Conflict of interest The authors report no declarations of interest.

References

1. Hwangbo, M., Claycomb, E.C., Liu, Y., Alivio, T.E., Banerjee, S., Chu, K.H.: Effectiveness of zinc oxide-assisted photocatalysis for concerned constituents in reclaimed wastewater: 1,4-Dioxane, trihalomethanes, antibiotics, antibiotic resistant bacteria (ARB), and antibiotic resistance genes (ARGs). Sci. Total Environ. **649**, 1189–1197 (2019)
2. Wang, G., Zhang, L., Li, Y., Zhao, W., Kuang, A., Li, Y., Xia, L., Li, Y., Xiao, S.: Biaxial strain tunable photocatalytic properties of 2D ZnO/GeC heterostructure. J. Phys. D. Appl. Phys. **53**, 015104 (2020)
3. Jin, S.E., Jin, J.E., Hwang, W., Hong, S.W.: Photocatalytic antibacterial application of zinc oxide nanoparticles and self-assembled networks under dual UV irradiation for enhanced disinfection. Int. J. Nanomedicine. **14**, 1737–1751 (2019)
4. Shanmugam, V., Sanjeevamuthu, S., Jeyaperumal, K.S., Vairamuthu, R.: Fabrication of heterostructured vanadium modified g-C 3 N 4 /TiO 2 hybrid photocatalyst for improved photocatalytic performance under visible light exposure and antibacterial activities. J. Ind. Eng. Chem. **76**, 318–332 (2019)
5. Qi, K., Cheng, B., Yu, J., Ho, W.: Review on the improvement of the photocatalytic and antibacterial activities of ZnO. J. Alloys Compd. **727**, 792–820 (2017)
6. Shanmugam, V., Jeyaperumal, K.S.: Investigations of visible light driven Sn and Cu doped ZnO hybrid nanoparticles for photocatalytic performance and antibacterial activity. Appl. Surf. Sci. **449**, 617–630 (2018)
7. Andrade, M.B., Guerra, A.C.S., Santos, T.R.T., Mateus, G.A.P., Bergamasco, R.: Innovative adsorbent based on graphene oxide decorated with Fe2O3/ZnO nanoparticles for removal of dipyrone from aqueous medium. Mater. Lett. **238**, 233–236 (2019)
8. Kulkarni, R.M., Malladi, R.S., Hanagadakar, M.S.: Cu-ZnO nanoparticles for degradation of methyl orange photocatalytic. Adv. Mater. Proc. **3**, 521–525 (2018)
9. Karuppaiah, S., Annamalai, R., Muthuraj, A., Kesavan, S., Palani, R., Ponnusamy, S., Nagarajan, E.R., Meenakshisundaram, S.: Efficient photocatalytic degradation of ciprofloxacin and bisphenol A under visible light using Gd2WO6 loaded ZnO/bentonite nanocomposite. Appl. Surf. Sci. **481**, 1109–1119 (2019)
10. Mohamed, R.M., McKinney, D., Kadi, M.W., Mkhalid, I.A., Sigmund, W.: Platinum/zinc oxide nanoparticles: enhanced photocatalysts degrade malachite green dye under visible light conditions. Ceram. Int. **42**, 9375–9381 (2016)
11. Choi, J., Chan, S., Joo, H., Yang, H., Ko, F.K.: Three-dimensional (3D) palladium-zinc oxide nanowire nanofiber as photo-catalyst for water treatment. Water Res. **101**, 362–369 (2016)
12. Sorbiun, M., Shayegan, M.E., Ramazani, A., Taghavi, F.S.: Biosynthesis of Ag, ZnO and bimetallic Ag/ZnO alloy nanoparticles by aqueous extract of oak fruit hull (Jaft) and investigation of photocatalytic activity of ZnO and bimetallic Ag/ZnO for degradation of basic violet 3 dye. J. Mater. Sci. Mater. Electron. **29**, 2806–2814 (2018)
13. Lu, J., Wang, H., Peng, D., Chen, T., Dong, S., Chang, Y.: Synthesis and properties of Au/ZnO nanorods as a plasmonic photocatalyst. Phys. E Low-Dimens. Syst. Nanostructures. **78**, 41–48 (2016)
14. Shanmugam, V., Muppudathi, A.L., Jayavel, S., Jeyaperumal, K.S.: Construction of high efficient g-C3N4 nanosheets combined with Bi2MoO6-Ag photocatalysts for visible-light-driven photocatalytic activity and inactivation of bacterias. Arab. J. Chem. **13**, 2439–2455 (2020)
15. Güy, N., Özacar, M.: The influence of noble metals on photocatalytic activity of ZnO for Congo red degradation. Int. J. Hydrogen Energy. **41**, 20100–20112 (2016)

16. Vignesh, S., Suganthi, S., Kalyana, S.J., Raj, V., Indra Devi, P.R.: Highly efficient visible light photocatalytic and antibacterial performance of PVP capped Cd:Ag: ZnO photocatalyst nanocomposites. Appl. Surf. Sci. **479**, 914–929 (2019)
17. Meshram, S.P., Adhyapak, P.V., Amalnerkar, D.P., Mulla, I.S.: Cu doped ZnO microballs as effective sunlight driven photocatalyst. Ceram. Int. **42**, 7482–7489 (2016)
18. Khan, H.R., Murtaza, G., Choudhary, M.A., Ahmed, Z., Malik, M.A.: Photocatalytic removal of carcinogenic reactive red S3B dye by using ZnO and Cu doped ZnO nanoparticles synthesized by polyol method: a kinetic study. Sol. Energy. **173**, 875–881 (2018)
19. Wu, J., Luo, C., Li, D., Fu, Q., Pan, C.: Preparation of Au nanoparticle-decorated ZnO/NiO heterostructure via nonsolvent method for high-performance photocatalysis. J. Mater. Sci. **52**, 1285–1295 (2017)
20. Seku, K., Gangapuram, B.R., Pejjai, B., Kadimpati, K.K., Golla, N.: Microwave-assisted synthesis of silver nanoparticles and their application in catalytic, antibacterial and antioxidant activities. J. Nanostructure Chem. **8**, 179–188 (2018)
21. Shanmugam, V., Jeyaperumal, K.S., Mariappan, P., Muppudathi, A.L.: Fabrication of novel g-C3N4based MoS2and Bi2O3nanorod embedded ternary nanocomposites for superior photocatalytic performance and destruction of bacteria. New J. Chem. **44**, 13182–13194 (2020)
22. Qi, K., Xing, X., Zada, A., Li, M., Wang, Q., Liu, S.Y., Lin, H., Wang, G.: Transition metal doped ZnO nanoparticles with enhanced photocatalytic and antibacterial performances: experimental and DFT studies. Ceram. Int. **46**, 1494–1502 (2020)
23. Abdel Messih, M.F., Ahmed, M.A., Soltan, A., Anis, S.S.: Synthesis and characterization of novel Ag/ZnO nanoparticles for photocatalytic degradation of methylene blue under UV and solar irradiation. J. Phys. Chem. Solids. **135**, 109086 (2019)
24. Phuruangrat, A., Wongwiwat, N., Thongtem, T., Thongtem, S.: Microwave-assisted solution synthesis and photocatalytic activity of Ag nanoparticles supported on ZnO nanostructure flowers. Res. Chem. Intermed. **44**, 7427–7436 (2018)
25 Swarnavalli, G.C.J., Dinakaran, S., Krishnaveni, S., Bhalerao, G.M.: Rapid one pot synthesis of Ag/ZnO nanoflowers for photocatalytic degradation of nitrobenzene. Mater. Sci. Eng. B Solid-State Mater. Adv. Technol. **247**, 114376 (2019)
26. Akram, M., Alshemary, A.Z., Butt, F.K., Goh, Y., Aini, W., Ibrahim, W., Hussain, R.: Continuous microwave flow synthesis and characterization of nanosized tin oxide. Mater. Lett. **160**, 146–149 (2015)
27. Dąbrowska, S., Chudoba, T., Wojnarowicz, J., Łojkowski, W.: Current trends in the development of microwave reactors for the synthesis of nanomaterials in laboratories and industries: a review. Crystals. **2017**, 1–26 (2018)
28. Akram, M., Butt, F.K., Alshemary, A.Z., Goh, Y., Aini, W., Ibrahim, W., Hussain, R.: Continuous microwave flow synthesis (CMFS) of nanosizedtitania: structural, optical and photocatalytic properties. Mater. Lett. **158**, 95–98 (2015)
29. Zhang, J., Gong, C., Zeng, X., Xie, J.: Continuous flow chemistry: new strategies for preparative inorganic chemistry. Coord. Chem. Rev. **324**, 39–53 (2016)
30. Nikam, A.V., Dadwal, A.H.: Scalable microwave-assisted continuous flow synthesis of CuO nanoparticles and their thermal conductivity applications as nanofluids. Adv. Powder Technol. **30**, 13–17 (2019)
31. Długosz, O., Banach, M.: Continuous synthesis of metal and metal oxide nanoparticles in microwave reactor. Colloids Surf. A Physicochem. Eng. Asp. **606**, 125453 (2020)
32. Monshi, A., Foroughi, M.R., Monshi, M.R.: Modified Scherrer equation to estimate more accurately nano-crystallite size using XRD. Artic. World J. Nano Sci. Eng. **2**, 154–160 (2012)
33. Barreto, G.P., Morales, G., Quintanilla, M.L.L.: Microwave assisted synthesis of ZnO nanoparticles: effect of precursor reagents, temperature, irradiation time, and additives on nano-ZnO morphology development. J. Mater. **2013**, 1–11 (2013)
34. Ferraris, S., Spriano, S., Miola, M., Bertone, E., Allizond, V., Cuffini, A.M., Banche, G.: Surface modification of titanium surfaces through a modified oxide layer and embedded silver nanoparticles: effect of reducing/stabilizing agents on precipitation and properties of the nanoparticles. Surf. Coat. Technol. **344**, 177–189 (2018)
35. Díaz-Cruz, C., Alonso, N.G., Espinoza-Gómez, H., Flores-López, L.Z.: Effect of molecular weight of PEG or PVA as reducing-stabilizing agent in the green synthesis of silver-nanoparticles. Eur. Polym. J. **83**, 265–277 (2016)
36. Cheng, Y., Wang, F., Fang, C., Su, J., Yang, L.: Preparation and characterization of size and morphology controllable silver nanoparticles by citrate and tannic acid combined reduction at a low temperature. J. Alloys Compd. **658**, 684–688 (2016)
37. Kadam, A.N., Kim, T.G., Shin, D.S., Garadkar, K.M., Park, J.: Morphological evolution of Cu doped ZnO for enhancement of photocatalytic activity. J. Alloys Compd. **710**, 102–113 (2017)
38. Babar, S.B., Gavade, N.L., Park, J., Garadkar, K.M., Bhuse, V.M.: Effect of leavening agent on structural and photocatalytic properties of ZnO nanorods. J. Mater. Sci. Mater. Electron. **28**, 8372–8381 (2017)
39. Saravanakumar, K., Muthuraj, V.: Fabrication of sphere like plasmonic Ag/SnO2 photocatalyst for the degradation of phenol. Optik (Stuttg). **131**, 754–763 (2017)
40. Rajar, K., Soomro, R.A., IbupotoSirajuddin, Z.H., Balouch, A.: Tannic acid assisted copper oxide nanoglobules for sensitive electrochemical detection of bisphenol A. Int. J. Food Prop. **20**, 1359–1367 (2017)
41. Ranoszek-Soliwoda, K., Tomaszewska, E., Socha, E., Krzyczmonik, P., Ignaczak, A., Orlowski, P., Krzyzowska, M., Celichowski, G., Grobelny, J.: The role of tannic acid and sodium citrate in the synthesis of silver nanoparticles. J. Nanoparticle Res. **19**, 273–288 (2017)
42. Agarwal, H., Nakara, A., Menon, S., Shanmugam, V.K.: Eco-friendly synthesis of zinc oxide nanoparticles using CinnamomumTamala leaf extract and its promising effect towards the antibacterial activity. J. Drug Deliv. Sci. Technol. **53**, 101212 (2019)
43. Khademalrasool, M., Farbod, M., Iraji, Z.A.: Preparation of ZnO nanoparticles/Ag nanowires nanocomposites as plasmonic photocatalysts and investigation of the effect of concentration and diameter size of Ag nanowires on their photocatalytic performance. J. Alloys Compd. **664**, 707–714 (2016)
44. Sriram, S., Lalithambika, K.C., Thayumanavan, A.: Experimental and theoretical investigations of photocatalytic activity of Cu doped ZnO nanoparticles. Optik (Stuttg). **139**, 299–308 (2017)
45. Karimi-Maleh, H., Kumar, B.G., Rajendran, S., Qin, J., Vadivel, S., Durgalakshmi, D., Gracia, F., Soto-Moscoso, M., Orooji, Y., Karimi, F.: Tuning of metal oxides photocatalytic performance using Ag nanoparticles integration. J. Mol. Liq. **314**, 113588 (2020)
46. Fageria, P., Gangopadhyay, S., Pande, S.: Synthesis of ZnO/Au and ZnO/Ag nanoparticles and their photocatalytic application using UV and visible light. RSC Adv. **4**, 24962–24972 (2014)
47. Fouda, A., Salem, S.S., Wassel, A.R., Hamza, M.F., Shaheen, T.I.: Optimization of green biosynthesized visible light active CuO/ZnO nano-photocatalysts for the degradation of organic methylene blue dye. Heliyon. **6**, 04896 (2020)

48. Isai, K.A., Shrivastava, V.S.: Photocatalytic degradation of methylene blue using ZnO and 2%Fe–ZnO semiconductor nanomaterials synthesized by sol–gel method: a comparative study. SN Appl. Sci. **1**, 1–11 (2019)
49. Lu, J., Batjikh, I., Hurh, J., Han, Y., Ali, H., Mathiyalagan, R., Ling, C., Ahn, J.C., Yang, D.C.: Photocatalytic degradation of methylene blue using biosynthesized zinc oxide nanoparticles from bark extract of Kalopanax septemlobus. Optik (Stuttg). **182**, 980–985 (2019)
50. Bomila, R., Srinivasan, S., Gunasekaran, S., Manikandan, A.: Enhanced photocatalytic degradation of methylene blue dye, optomagnetic and antibacterial behaviour of pure and la-doped ZnO nanoparticles. J. Supercond. Nov. Magn. **31**, 855–864 (2018)
51. Atchudan, R., Edison, T.N., Perumal, S., Karthikeyan, D., Lee, Y.R.: Facile synthesis of zinc oxide nanoparticles decorated graphene oxide composite via simple solvothermal route and their photocatalytic activity on methylene blue degradation. J. Photochem. Photobiol. B Biol. **162**, 500–510 (2016)
52. Asgharian, M., Mehdipourghazi, M., Khoshandam, B., Keramati, N.: Photocatalytic degradation of methylene blue with synthesized rGO/ZnO/Cu. Chem. Phys. Lett. **719**, 1–7 (2019)
53. Lee, S.J., Jung, H.J., Koutavarapu, R., Lee, S.H., Arumugam, M., Kim, J.H., Choi, M.Y.: ZnO supported Au/Pd bimetallic nanocomposites for plasmon improved photocatalytic activity for methylene blue degradation under visible light irradiation. Appl. Surf. Sci. **496**, 143665 (2019)
54. Shah, A.A., Bhatti, M.A., Tahira, A., Chandio, A.D., Channa, I.A., Sahito, A.G., Chalangar, E., Willander, M., Nur, O., Ibupoto, Z.H.: Facile synthesis of copper doped ZnO nanorods for the efficient photo degradation of methylene blue and methyl orange. Ceram. Int. **46**, 9997–10005 (2020)
55. Ahmed, M.A., Abou-Gamra, Z.M., ALshakhanbeh, L.A., Medien, H.: Control synthesis of metallic gold nanoparticles homogeneously distributed on hexagonal ZnO nanoparticles for photocatalytic degradation of methylene blue dye. Environ. Nanotechnol. Monit. Manag. **12**, 100217 (2019)
56. Pathak, T.K., Kroon, R.E., Swart, H.C.: Photocatalytic and biological applications of Ag and Au doped ZnO nanomaterial synthesized by combustion. Vacuum **157**, 508–513 (2018)
57. Lam, S.M., Quek, J.A., Sin, J.C.: Mechanistic investigation of visible light responsive Ag/ZnO micro/nanoflowers for enhanced photocatalytic performance and antibacterial activity. J. Photochem. Photobiol. A Chem. **353**, 171–184 (2018)
58. Xiong, J., Sun, Q., Chen, J., Li, Z., Dou, S.: Ambient controlled synthesis of advanced core-shell plasmonic Ag@ZnO photocatalysts. CrystEngComm **18**, 1713–1722 (2016)
59. Adeleke, J.T., Theivasanthi, T., Thiruppathi, M., Swaminathan, M., Akomolafe, T., Alabi, A.B.: Photocatalytic degradation of methylene blue by ZnO/NiFe2O4 nanoparticles. Appl. Surf. Sci. **455**, 195–200 (2018)
60. Uribe López, M.C., Alvarez Lemus, M.A., Hidalgo, M.C., López, G.R., Quintana, O.P., Oros-Ruiz, S., Uribe López, S.A., Acosta, J.: Synthesis and characterization of ZnO-ZrO2 nanocomposites for photocatalytic degradation and mineralization of phenol. J. Nanomater. **2019**, 1–12 (2019)